

# Synthesis and characterization of uniform spherical shape nanoparticles of indium oxide

S. C. Kulkarni<sup>1</sup> · D. S. Patil<sup>1</sup>

Received: 7 September 2015 / Accepted: 9 December 2015 / Published online: 18 December 2015  
© Springer Science+Business Media New York 2015

**Abstract** Spherical shape nanoparticles of indium oxide ( $\text{In}_2\text{O}_3$ ) has been synthesized by simple and cost effective sol gel method with indium nitrate hydrate as a precursor. The nanoparticles were characterized by X-ray diffraction, Fourier transform infra red spectroscopy (FTIR) and transmission electron microscopy (TEM). Morphological observations showed a uniform size distribution of spherical particles. From TEM, spherical particles size was found to vary from 17 to 23 nm. The most number of the nanoparticles out of total were 17 nm in size. The absorption spectra in ultraviolet region of  $\text{In}_2\text{O}_3$  showed optical band gap of 3.6 eV. FTIR study reveals that the nanoparticles are single phase cubic structure of  $\text{In}_2\text{O}_3$ . Photo-luminescence spectrum at room temperature showed peak at 347 nm in ultraviolet region.

## 1 Introduction

Indium oxide ( $\text{In}_2\text{O}_3$ ) has been investigated extensively for its semiconducting properties. It is an important and well known transparent conducting oxide (TCO) over past decades. It shows the unusual combination of high transparency in the visible region and possesses high electrical conductivity. These properties signify  $\text{In}_2\text{O}_3$  for a number of potential applications such as solar cells, optoelectronic devices and liquid crystal displays.  $\text{In}_2\text{O}_3$  has two phases: cubic  $\text{In}_2\text{O}_3$  (c- $\text{In}_2\text{O}_3$ ) and hexagonal  $\text{In}_2\text{O}_3$  (h- $\text{In}_2\text{O}_3$ ). A c- $\text{In}_2\text{O}_3$  nanomaterial has attracted more and more attention

due to its high sensitivity.  $\text{In}_2\text{O}_3$  is promising candidate for gas sensing applications [1] and nanoscale  $\text{In}_2\text{O}_3$  shows superior sensing properties [2, 3]. Semiconductor nanostructures have been extensively studied in last decade because of their exceptional properties, which differ from those of their bulk counterparts. Research on nanostructures provides the potential for a variety of chemical, electronic, catalytic, electrochemical and photonic applications [4–6].

The technological utility of  $\text{In}_2\text{O}_3$  has promoted considerable interest in the development of synthesis techniques that are capable of manufacturing nanoparticles of  $\text{In}_2\text{O}_3$  powder with a controlled particle size. To synthesize nanocrystalline  $\text{In}_2\text{O}_3$  using cheap, nontoxic and environmentally benign, precursors are still key issue. In recent years, many methods such as co-precipitation method and thermal evaporation method [7], non-aqueous sol-gel method [8], CVD route [9], glass crystallization [10], hydro/solvothermal [11, 12], and microemulsion-mediated hydrothermal synthesis [13] have been used for preparing different shapes of  $\text{In}_2\text{O}_3$  nanostructures [14–16]. All these methods resulted in production of  $\text{In}_2\text{O}_3$  particles with different sizes and morphologies.

The sol-gel is considered as the most promising technique for preparation of metal oxide nanoparticles because it has numerous comparative advantages over other synthesis techniques such as ease of preparation, purity, stoichiometric control, homogeneity, ease of introducing dopants, ability to produce thin film coatings, fibers, porous powders and self supported bulk structure [17, 18]. Omri et al. [19] reported synthesis of hexagonal wurtzite structure of ZnO nanoparticles with particle size 35–54 nm using sol-gel method. Aziz et al. [20] reported size-controlled synthesis of  $\text{SnO}_2$  nanoparticles by sol-gel method. Karami [21] synthesized titanium dioxide nano powder with particle sizes 12–20 nm and pure anatase titanium

✉ D. S. Patil  
patildsp@rediffmail.com

<sup>1</sup> Department of Electronics, North Maharashtra University, Jalgaon, Maharashtra, India

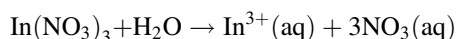
dioxide was obtained by adjusting gel pH to value of 3. This sol–gel synthesized material have better photocatalytic reactivity than reference material employed. Omri et al. [22] studied Mn doped ZnO nanoparticles with different doping concentration (1, 2, 3, 4, 5 at.%) which were prepared by sol–gel method. The structural properties showed that the undoped and Mn doped ZnO nanoparticles exhibit hexagonal wurtzite structure. The optical and magnetic properties changes with % change in doping concentration.

Although above mentioned metal oxide semiconductors nano particles [19–21] have been obtained using sol–gel method, some improvement is still needed to obtain pure and homogenous nanoparticles of small particle size at lower temperature with minimum reaction time. Here, we report the synthesis of In<sub>2</sub>O<sub>3</sub> nanoparticles at low temperature and minimum reaction time without any surfactants. In this work, c-In<sub>2</sub>O<sub>3</sub> nanocrystalline spherical shape particles of size 17–23 nm were synthesized by facile cost effective chemical route. We have investigated the structural and micro structural properties of In<sub>2</sub>O<sub>3</sub>. The UV–visible absorption spectroscopy was utilized to deduce band gap which matches with reported value. Photoluminescence of In<sub>2</sub>O<sub>3</sub> nanocrystalline particles were studied which showed emission in UV region.

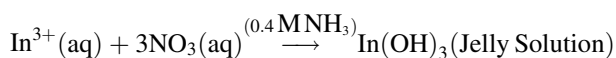
The main goal of the paper is to present uniform spherical size nanoparticles of In<sub>2</sub>O<sub>3</sub> having size about 17 nm. The following section of paper discusses the experimental procedure used for the synthesis of the nanoparticles followed by results and discussions. Finally, conclusions are highlighted.

## 2 Experimental

Indium (III) Nitrate hydrate (In(NO<sub>3</sub>)<sub>3</sub>) (2.5 gm) (Aldrich metal basis 99.9 %), was added in 60 ml bi-distilled water to prepare aqueous solution of Indium Nitrate hydroxide. Solution was stirred until it becomes clear.



Ammonia (0.4 M) solution was added drop wise to Indium Nitrate hydrate solution to adjust pH until 9 while stirring. A precipitate was observed immediately. However, stirring was continued for 30 min.



This solution was centrifuged for half an hour at 5000 rpm (using REMI R-24) to separate the precipitate which was then washed with bi-distilled water and methanol several times to remove any excess ammonia ion. The white precipitate was sintered at 400 °C for an hour in air ambient using muffle furnace. This calcinations temperature was

chosen due to the complete phase transformation from In(OH)<sub>3</sub> into In<sub>2</sub>O<sub>3</sub> and complete removal of N-radicals. At this calcinations temperature, white precipitate was turned into yellowish colored In<sub>2</sub>O<sub>3</sub> nanocrystalline powder. The obtained yield was 0.88 gm.

Information about the crystallinity and crystal phases of the calcined powder was obtained using X-ray diffraction (XRD, Bruker D8, Advance) spectroscopy with Cu-K $\alpha$  Radiation ( $\lambda = 1.542 \text{ \AA}$ ) for the Bragg angle ranging from 20° to 80°. The phase of the Nanocrystalline particles were confirmed by using XRD and particle size was determined by using Scherrer formula

$$D = \frac{0.9\lambda}{\beta \cos\theta}$$

where,  $D$  is the average grain size,  $\lambda = 1.541 \text{ \AA}$ , the wavelength of X-ray radiation used and  $\beta$  is the angular width of the diffraction peak at the half maximum (FWHM) for diffraction angle  $2\theta$ .

Optical properties of In<sub>2</sub>O<sub>3</sub> were studied using UV–visible spectroscopy (JASCO V-670). The morphologies and dimensions of the nanoparticles were observed by transmission electron microscopy (TEM). TEM image, high resolution transmission electron microscope (HRTEM) image, and selected area electron diffraction (SAED) pattern were obtained using Philips CM-200 with accelerating voltage 200 kV. Fourier transform infra red spectroscopy (FTIR) spectra of powders were recorded over range 400–4000 cm<sup>-1</sup> using (JASCO-650) KBr pellet method. Photoluminescence (PL) measurement was carried out using F-2500 FL Spectrofluorometer.

## 3 Results and discussion

Figure 1 shows XRD pattern of calcinated In<sub>2</sub>O<sub>3</sub> Nanocrystalline particles. Diffraction pattern of Nanocrystalline particles closely matched with c-In<sub>2</sub>O<sub>3</sub> (JCPDS card

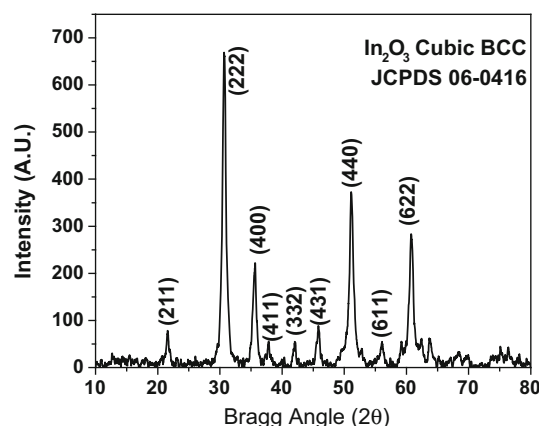


**Fig. 1** X-ray diffraction spectra of In<sub>2</sub>O<sub>3</sub> nanoparticles

number 06-0416). This confirms that synthesis is viable and complete producing high quality  $\text{In}_2\text{O}_3$  nanocrystalline particles (impurity free, with X-ray detection limits). The preferentially oriented crystal plane was found to be (222) for the particles prepared using sol gel technique. The sharp diffraction peaks for the sample indicate a high degree of crystallization. The lattice constant of powder were calculated from XRD peaks by indexing it in a cubic space group Ia  $\sim$  3 using least square refinement (Ia  $\sim$  3 space group with lattice parameter  $a = b = c = 10.117 \text{ \AA}$ ). The XRD pattern indicates formation of crystalline  $\text{In}_2\text{O}_3$  particles with base centered cubic (BCC) structure with average crystallite size of 15 nm (estimated from Scherrer formula). The UV–visible absorption spectra of  $\text{In}_2\text{O}_3$  samples show well defined absorption peak at 293 nm (4.23 eV). The direct band gap energy ( $E_g$ ) of sample has been deduced by fitting absorption data to direct transition equation

$$\alpha h\nu = E_D (h\nu - E_g)^{1/2}$$

where,  $\alpha$  is absorption coefficient,  $h\nu$  is photon energy,  $E_g$  is direct band gap and  $E_D$  is constant [23]. Plotting  $(\alpha h\nu)^2$  as a function of photon energy and extrapolating linear portion of curve to absorption equal to zero has been illustrated in inset of Fig. 2. The direct band gap ( $E_g$ ) deduced from this plot was found to be 3.6 eV. This value of optical band gap exactly matches with reported value [24].

Figure 3 depicts the TEM image of calcinated  $\text{In}_2\text{O}_3$  and corresponding SAED pattern. The particles were mostly spherical in shape. The particles size was observed which vary from 17 to 23 nm. The corresponding SAED of  $\text{In}_2\text{O}_3$  sample show spotty ring pattern without any additional diffraction spot and rings of second phases, revealing their crystalline cubic structure along (222) plane. The measured

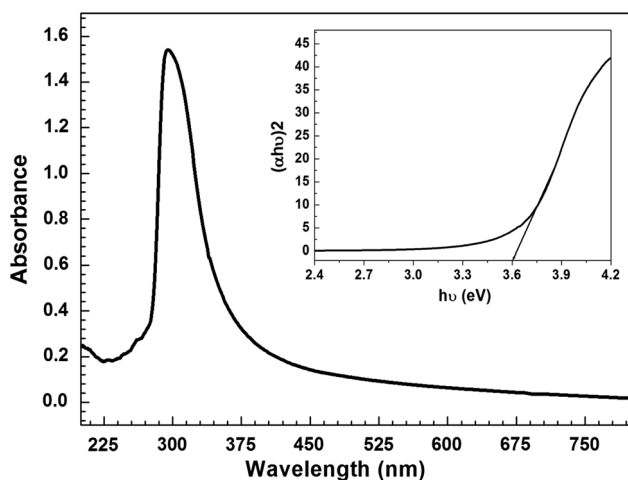


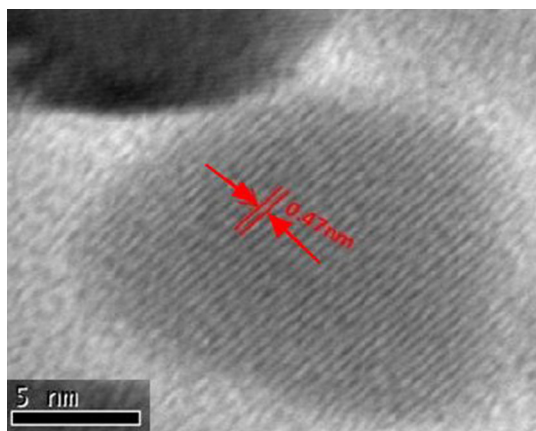
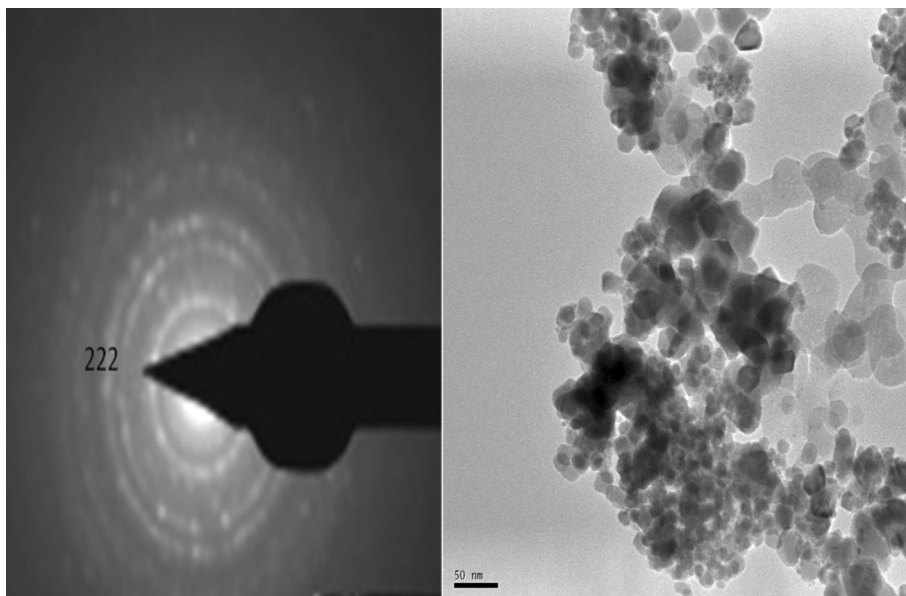
**Fig. 2** UV–visible spectra of  $\text{In}_2\text{O}_3$  nanoparticles

interplanar spacing  $d(hkl)$  from SAED pattern shows (211), (222), (400), (411), (332), (431) and (440) reflections which corresponds to cubic phase of  $\text{In}_2\text{O}_3$  nanocrystalline material and there by matching with XRD pattern (JCPDS card number 06-0416). Figure 4 shows HRTEM image of  $\text{In}_2\text{O}_3$  nanoparticles having perfectly crystallized particles in the form of single crystals, as demonstrated by the lattice planes that clearly mark the particle boundaries. The particles were mostly in spherical shape and agglomerated. Particle size distribution has been carried out by using dynamic light scattering techniques (DLS) via Laser input energy of 632 nm. Figure 5 explores particle size distribution curve of  $\text{In}_2\text{O}_3$  nanoparticles. The volume/wt analysis of sample gave distribution of particle size between 17 and 23 nm in case of  $\text{In}_2\text{O}_3$  nanoparticles. It was observed that particles of  $\text{In}_2\text{O}_3$  have narrow size distribution within range of 6 nm. The most of the particles showed size of 17 nm.

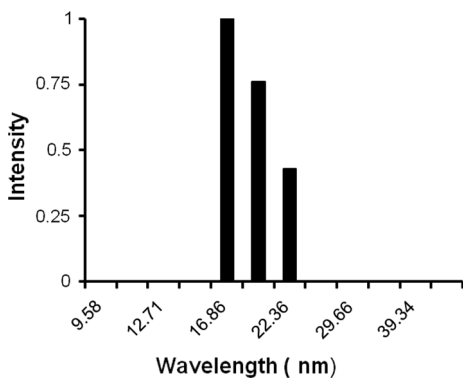
Figure 6 reveals the IR spectra of calcinated powder at 400 °C. The appearance of peaks at 406, 428.96, 501.28 and 590.56  $\text{cm}^{-1}$  correspond to the In–O phonon vibration mode and characteristics of c- $\text{In}_2\text{O}_3$  [25, 26]. The large absorption band at around 3447.50  $\text{cm}^{-1}$  shows OH stretching. The peak at 2347.07  $\text{cm}^{-1}$  has been attributed to absorption of  $\text{CO}_2$  [27]. The absorption bands at 1340.52, 1507.72 and 1636.30  $\text{cm}^{-1}$  were assigned to nitrate group and shows bend deformation of water [28]. A minor vibration in their frequencies or relative intensities occurs in different  $\text{In}^{3+}$  distributions in the interstitial sites. They are sensitive to oxygen vacancies and other defects [29]. This result reveals that the phase formation is complete and there is no evidence for presence of any organic intermediates in sample.

Figure 7 represents the room temperature PL spectra of Nanocrystalline  $\text{In}_2\text{O}_3$  sample using a Xenon laser of 250 nm as an excitation source. Though bulk  $\text{In}_2\text{O}_3$  could not emit light, its nanostructure can emit visible and UV light [30]. The spectra of sample mainly consist of a strong UV emission broad band having emission peak at 347 nm (3.6 eV). PL emission in  $\text{In}_2\text{O}_3$  sample is due to effect of oxygen vacancies as reported in literature [31–33]. The oxygen vacancies would generally act as deep defect donors and cause the formation of new energy levels in the band gap of  $\text{In}_2\text{O}_3$  samples. Small  $\text{In}_2\text{O}_3$  particles would favor the existence of oxygen vacancies as found in  $\text{In}_2\text{O}_3$  nanowires with high surface to volume ratio [34]. The PL emission from  $\text{In}_2\text{O}_3$  nanoparticles having electron occupying oxygen vacancies with a photo excited hole is analogous mechanism in ZnO and  $\text{SnO}_2$  semiconductors [35, 36]. Presence of oxygen vacancies in the material is a good sign for sensing applications, where free electrons will occupy the vacancy sites which act as adhesion sites to gases.

**Fig. 3** TEM image and SAED pattern of In<sub>2</sub>O<sub>3</sub> nanoparticles



**Fig. 4** HRTEM image of In<sub>2</sub>O<sub>3</sub> nanoparticles



**Fig. 5** Particle size distribution of In<sub>2</sub>O<sub>3</sub> nanoparticles by using DLS

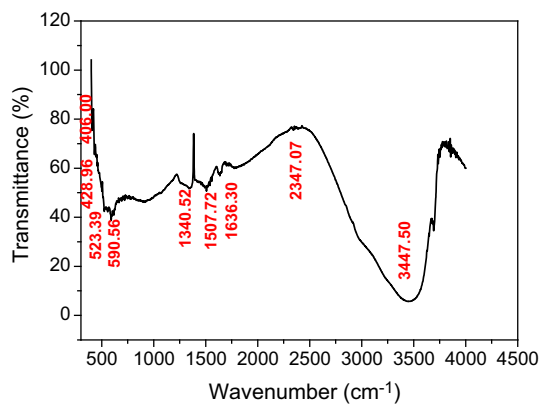


**Fig. 6** FTIR analysis of In<sub>2</sub>O<sub>3</sub> nanoparticles calcined at 400 °C

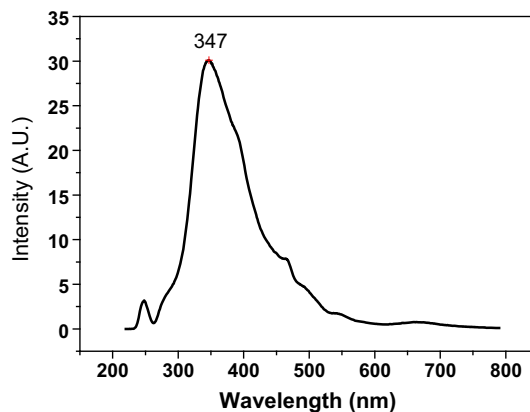


**Fig. 7** PL spectra of synthesized In<sub>2</sub>O<sub>3</sub> nanoparticles at room temperature

## 4 Conclusion

Nanocrystalline  $\text{In}_2\text{O}_3$  has been successfully synthesized using cost effective chemical route technique of sol gel. XRD and TEM analysis showed that  $\text{In}_2\text{O}_3$  samples are cubic in nature. FTIR study clearly explores the complete phase formation and peak observed was characteristics of the c- $\text{In}_2\text{O}_3$  phase. The optical band gap value was 3.6 eV which shows excellent consistency with reported value. TEM and HRTEM showed uniform spherical distribution of nanocrystalline particles with size 17–23 nm. PL spectra with excited wavelength of 250 nm showed emission in UV region with peak at 347 nm. The sol–gel technique used here is characterized by fine control of PH. We were successful in achieving uniform spherical shaped nanoparticles of size 17 nm for its potential for gas sensing.

**Acknowledgments** S. C. Kulkarni thanks University Grant Commission (UGC) for awarding teacher fellowship under Faculty Improvement Program (F.I.P.). Authors acknowledge P. K. Khanna, Nanoscience Laboratory, C-MET, Pune for his valuable co-operation during synthesis.

## References

1. S.C. Kulkarni, D.S. Patil, *Sens. Lett.* **13**, 294 (2015)
2. M. Ivanovskaya, A. Gurlo, P. Bogdanov, *Sens. Actuators B* **77**, 264 (2001)
3. S.C. Kulkarni, C.S. Aher, R.Y. Borse, B.G. Bharate, S.S. Al-Deyab, S.G. Ansari, P.K. Khanna, *Adv. Sci. Lett.* **5**, 109 (2012)
4. P.P. George, A. Gedanken, *Eur. J. Inorg. Chem.* **6**, 919 (2008)
5. E.C.C. Souza, J.F.Q. Rey, E.N.S. Muccillo, *Appl. Surf. Sci.* **255**, 3779 (2009)
6. A. Gurlo, M. Ivanovskaya, A. Pfau, U. Weimer, W. Gopel, *Thin Solid Films* **307**, 288 (1997)
7. J.M. Kim, J.K. Park, K.N. Kim, C.H. Kim, H.G. Jang, *Curr. Appl. Phys.* **6S1**, e198 (2006)
8. G. Neri, A. Bonavita, G. Micali, G. Rizzo, N. Pinna, M. Niederberger, *Sens. Actuator B* **127**, 455 (2007)
9. Y. Zhanga, H. Agoa, J. Liub, M. Yumuraa, K. Uchidaa, S. Ohshimaa, S. Iijimaa, J. Zhub, X. Zhang, *J. Cryst. Growth* **264**, 363 (2004)
10. R. Garkova, G. Volksch, C. Russel, *J. Non-Cryst. Solids* **352**, 5265 (2006)
11. Z. Yuan, J. Zhang, G. Liu, *Int. J. Electrochem. Sci.* **8**, 1794 (2013)
12. A. Askarinejad, M. Iranpour, N. Bahramifar, A. Morsali, *J. Exp. Nanosci.* **5**, 294 (2010)
13. J. Zhang, J. Hu, Z.Q. Zhu, H. Gong, S.J. O'Shea, *Colloids Surf. A* **236**, 23 (2004)
14. J. Yang, C. Lin, Z. Wang, J. Lin, *Inorg. Chem.* **45**, 8973 (2006)
15. S. Park, H. Ko, S. An, W. Lee, S. Lee, C. Lee, *Ceram. Int.* **39**, 5255–5262 (2013)
16. S.Y. Istomin, E.V. Antipov, Y.S. Fedotov, S.I. Bredikhin, N.V. Lyskov, S. Shafeie, G. Svensson, Y. Liu, Z. Shen, *J. Solid State Electrochem.* **18**, 1415–1423 (2014)
17. F. Li, J. Jian, W. Rong, J. Li, Y. Sun, *J. Alloys Compd.* **645**, 178–183 (2015)
18. R.B.H. Tahar, T. Ban, Y. Ohya, Y. Takahashi, *J. Appl. Phys.* **82**, 865 (1997)
19. K. Omri, I. Najeh, R. Dhahri, J. El Ghoul, L. El Mir, *Microelectron. Eng.* **128**, 53 (2014)
20. M. Aziz, S.S. Abbas, W.R.W. Baharom, *Mater. Lett.* **91**, 31–34 (2013)
21. A. Karami, *J. Iran. Chem. Soc.* **7**, s154–s160 (2010)
22. K. Omri, J. El Ghoul, O.M. Lemine, M. Bououdina, B. Zhang, L. El Mir, *Superlattices Microstruct.* **60**, 139 (2013)
23. E. Ziegler, A. Heinrich, H. Oppermann, G. Stover, *Phys. Status Solidi A* **66**, 635 (1981)
24. M.I. Ivanovskaya, E.A. Ovodok, D.A. Kotsikau, *Glass Phys. Chem.* **37**, 560 (2011)
25. S.K. Poznyak, A.N. Golubev, A.I. Kulak, *Surf. Sci.* **454**, 396 (2000)
26. J.W. Robinson, *Practical Handbook of Spectroscopy* (CRC Press, Florida, 2000), p. 533
27. J. Chandradass, K.S. Han, D. Sik Bae, *J. Mater. Sci. Technol.* **206**, 315 (2008)
28. V.N. Singh, B.R. Mehta, *Jpn. J. Appl. Phys.* **42**, 4226 (2003)
29. A. Mondal, S. Ram, *Ceram. Int.* **30**, 239 (2004)
30. M. Seetha, S. Bharathi, A.D. Raj, D. Mangalaraj, D. Nataraj, *Mater. Charact.* **60**, 1578 (2009)
31. J.S. Jeong, J.Y. Lee, C.J. Lee, S.J. An, G.-C. Yi, *Chem. Phys. Lett.* **384**, 246 (2004)
32. Q. Tang, W. Zhou, W. Zhang, S. Ou, K. Jiang, W. Yu, Y. Qian, *Cryst. Growth Des.* **5**, 147 (2005)
33. Y. Zhang, J. Li, Q. Li, L. Zhu, X. Liu, X. Zhong, J. Meng, X. Cao, *Scr. Mater.* **56**, 409 (2007)
34. M.S. Lee, W.C. Choi, E.K. Kim, C.K. Kim, S.K. Min, *Thin Solid Films* **279**, 1 (1996)
35. J. Zhang, X. Qing, F. Jiang, Z. Dai, *Chem. Phys. Lett.* **371**, 311 (2003)
36. C.H. Liang, G.W. Meng, Y. Lei, F. Phillipp, L.D. Zhang, *Adv. Mater.* **13**, 1330 (2001)